Supplementary material

RF-spoiled gradient echo	1 mm isotropic resolution FOV 25.6 x 25.6 cm^2 166 slices TE 2.9 ms, TR 7.6 ms 11^o flip angle
^{13}C-image acquisition	15 mm isotropic resolution FOV 24 x 24^2 24 slices 11^o flip angle for ^{13}C-pyruvate 80^o flip angle for ^{13}C-lactate 80^o flip angle for ^{13}C-bicarbonate
^{13}C-spectroscopy slab)	100 mm slab thickness 10^o flip angle 16384 samples at 32 kHz 512 ms acquisition time

Table 1: Scan parameters for T1-weighted anatomical images, ^{13}C-image acquisition and ^{13}C-spectroscopy slab acquisitions.

Let the regression coefficient for the effect of age on a log-transformed variable of interest be β_{age}, which gives the change in the log variable per year. This can be converted to a percentage change per decade of the anti-log-transformed variable, p_{decade}, as follows:

$$p_{decade} = (1 - e^{10\beta_{age}}) \times 100\% \quad [1]$$

Models compared with ANOVA for L_P	**p-value**
Brain region vs brain region + sex	0.2
Brain region vs brain region + weight	0.06
Brain region vs brain region + age	0.01
Brain region + age vs brain region + age + weight	0.09
Brain region + age vs brain region $*$ age	0.002
Brain region $*$ age vs brain region $*$ age + weight	0.09

Table 2: Example results from the iterative process used when mixed-effect model building for $\log(L_P)$. The p-value results from an ANOVA comparing the two listed models, with a significant p-value suggesting that the inclusion of an additional variable or interaction significantly improved the modelling of the observed variance. The first test suggested that biological sex should not be included. The same was found for the next model, which tested brain region versus both brain region and weight as independent fixed effects. This process resulted in the final model with age, region and an interaction (indicated by $*$) between age and region.

Models compared with ANOVA for B_P	**p-value**
Brain region vs brain region + sex	0.09
Brain region vs brain region + weight	0.1
Brain region vs brain region + age	0.009
Brain region + age vs brain region + age + weight	0.2
Brain region + age vs brain region $*$ age	$<$0.0001
Brain region $*$ age vs brain region $*$ age + weight	0.2

Table 3: Example results from the iterative process used when mixed-effect model building for $\log(B_P)$. The p-value results from an ANOVA comparing the two listed models, with a significant p-value suggesting that the inclusion of an additional variable or interaction significantly improved the modelling of the observed variance. The first test suggested that biological sex should not be included. The same was found for the next model, which tested brain region versus both brain region and weight as independent fixed effects. This process resulted in the final model with age, region and an interaction (indicated by $*$) between age and region.

Factor	**DFn**	**DFd**	**F**	**p**
Age (categorical)	1	33	12.5	0.001
Region	131	4323	42.9	< 0.0001
Age:Region	131	4323	1.2	0.04

Table 4: Mixed-effects ANOVA table for the log of the dependent variable L_P vs. age, region, and an age-region interaction term.

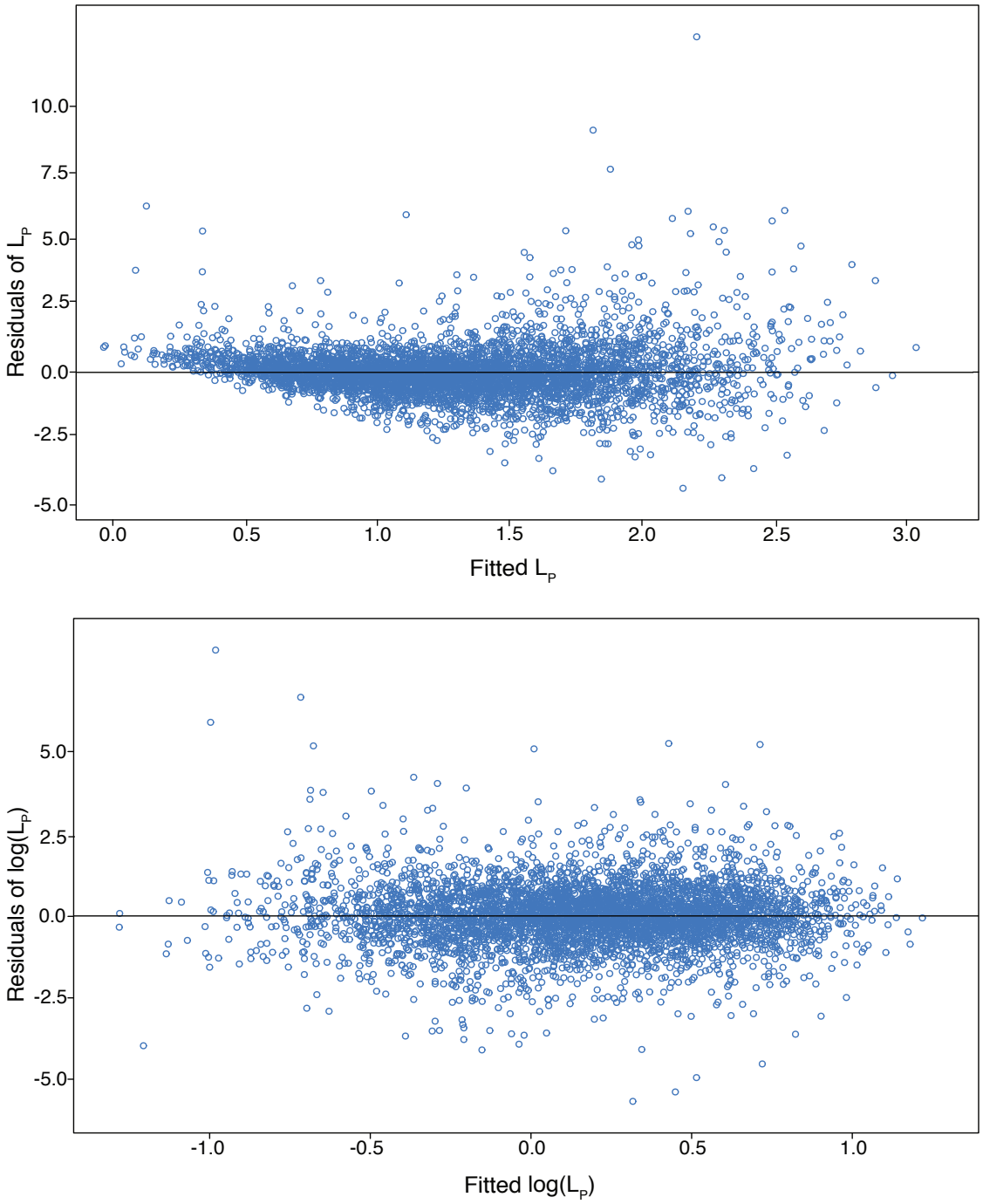

Figure S1: Transformation of L_P data to log-scale significantly improves heteroscedasticity in observed data. Residuals as a function of fitted values from the regression model using (a) the ratio L_P as the dependent variable and (b) using $\log(L_P)$. Heteroscedasticity, where variance of the residuals depends on L_P values, can be observed in (a) whereas taking the log of L_P achieves a homoscedastic distribution (b).

Factor	**DFn**	**DFd**	**F**	**p**
Age (categorical)	1	33	12.2	0.001
Region	131	4323	28.9	< 0.0001
Age:Region	131	4323	1.0	0.5

Table 5: Mixed-effects ANOVA table for log of the dependent variable B_P vs. age, region and an age-region interaction term.

Region	Estimate	t-statistic	p-value
R-POrG	-0.54	-4.5	0.00008
L-SCA	-0.53	-4.4	0.0001
L-AcA	-0.51	-4.3	0.0002
L-MCgG	-0.50	-4.1	0.0002
R-AntIns	-0.49	-4.1	0.0003
R-OrlFG	-0.49	-4.0	0.0003
L-Calc	-0.47	-3.9	0.0004
R-VentDC	-0.47	-3.9	0.0005
R-MPrG	-0.47	-3.9	0.0005
L-BasForbr	-0.46	-3.8	0.0006
CerebVermLob VII-X	-0.45	-3.7	0.0007
L-Ent	-0.45	-3.7	0.0007
L-AntIns	-0.45	-3.7	0.0008
R-MCgG	-0.44	-3.7	0.0009
L-OplFG	-0.44	-3.6	0.001
R-TrlFG	-0.44	-3.6	0.001
R-FO	-0.43	-3.6	0.001
L-FuG	-0.43	-3.5	0.001
L-POrG	-0.43	-3.5	0.001
L-TrlFG	-0.43	-3.5	0.001
4th Vent	-0.42	-3.5	0.001
L-MFC	-0.42	-3.5	0.001
L-Gre	-0.42	-3.5	0.001
L-PCgG	-0.42	-3.5	0.001
L-OrlFG	-0.42	-3.4	0.002
R-PCgG	-0.41	-3.4	0.002
L-Amyg	-0.41	-3.4	0.002
L-FO	-0.41	-3.4	0.002
L-Pins	-0.41	-3.4	0.002
R-PT	-0.40	-3.3	0.002
R-ThalProp	-0.40	-3.3	0.002
L-PO	-0.40	-3.3	0.002
L-PT	-0.40	-3.3	0.002
R-MOrG	-0.39	-3.3	0.003
L-VentDC	-0.39	-3.3	0.003
L-TTG	-0.39	-3.2	0.003
L-MOrG	-0.39	-3.2	0.003
L-CO	-0.38	-3.2	0.003
R-MPoG	-0.38	-3.2	0.003
L-OFuG	-0.38	-3.2	0.003
L-CerebelWM	-0.38	-3.2	0.003
R-LiG	-0.38	-3.2	0.003
R-CO	-0.38	-3.2	0.003
L-PHG	-0.38	-3.2	0.003

L-PP	-0.38	-3.2	0.003
R-TTG	-0.38	-3.2	0.003
CerebVermLob I-V	-0.38	-3.1	0.004
R-BasForbr	-0.37	-3.1	0.004
L-ITG	-0.37	-3.1	0.004
R-PP	-0.37	-3.1	0.004
R-Pins	-0.37	-3.0	0.005
L-CerebelEx	-0.37	-3.0	0.005
R-Pall	-0.37	-3.0	0.005
CerebVermLob VI-VII	-0.36	-3.0	0.005
L-LiG	-0.36	-3.0	0.005
L-TMP	-0.36	-3.0	0.005
R-TMP	-0.36	-3.0	0.006
R-SMC	-0.36	-2.9	0.006
L-Putam	-0.36	-2.9	0.006
R-Pcu	-0.36	-2.9	0.006
R-CerebelEx	-0.35	-2.9	0.006
R-LOrG	-0.35	-2.9	0.006
L-MPoG	-0.35	-2.9	0.006
3rd Vent	-0.35	-2.9	0.006
L-MPrG	-0.35	-2.9	0.006
R-MSFG	-0.35	-2.9	0.007
R-STG	-0.35	-2.9	0.007
R-OFuG	-0.35	-2.9	0.007
R-Putam	-0.34	-2.8	0.008
L-ACgG	-0.34	-2.8	0.008
L-PrG	-0.34	-2.8	0.009
R-Cun	-0.34	-2.8	0.009
L-Hc	-0.33	-2.7	0.010
L-CerebWM	-0.33	-2.7	0.01
R-OplFG	-0.33	-2.7	0.01
L-AnG	-0.33	-2.7	0.01
R-Amyg	-0.33	-2.7	0.01
L-STG	-0.32	-2.7	0.01
L-InfLatVent	-0.32	-2.7	0.01
L-ThalProp	-0.32	-2.6	0.01
R-AnG	-0.32	-2.6	0.01
R-ACgG	-0.32	-2.6	0.01
L-IOG	-0.32	-2.6	0.01
L-MSFG	-0.32	-2.6	0.01
R-PoG	-0.32	-2.6	0.01
R-CerebWM	-0.31	-2.6	0.01
R-SCA	-0.31	-2.6	0.01
R-PO	-0.31	-2.6	0.01
L-SMC	-0.31	-2.6	0.01

R-Calc	-0.31	-2.6	0.02
R-MFC	-0.31	-2.5	0.02
R-ITG	-0.31	-2.5	0.02
R-MOG	-0.31	-2.5	0.02
R-SOG	-0.30	-2.5	0.02
L-Cun	-0.30	-2.5	0.02
R-CerebelWM	-0.30	-2.5	0.02
R-Hc	-0.30	-2.5	0.02
R-SMG	-0.30	-2.5	0.02
Brainstem	-0.30	-2.5	0.02
L-SMG	-0.29	-2.4	0.02
R-IOG	-0.29	-2.4	0.02
R-Gre	-0.29	-2.4	0.02
L-AOrG	-0.29	-2.4	0.02
R-Ent	-0.28	-2.4	0.02
L-FRP	-0.28	-2.4	0.02
L-LOrG	-0.28	-2.3	0.03
R-PrG	-0.28	-2.3	0.03
L-Pcu	-0.28	-2.3	0.03
L-MFG	-0.28	-2.3	0.03
R-PHG	-0.27	-2.3	0.03
R-LatVent	-0.27	-2.3	0.03
L-MTG	-0.27	-2.2	0.03
R-MTG	-0.27	-2.2	0.03
R-FuG	-0.27	-2.2	0.03
L-LatVent	-0.27	-2.2	0.03
R-InfLatVent	-0.26	-2.2	0.04
L-SFG	-0.26	-2.2	0.04
L-SPL	-0.26	-2.2	0.04
L-Pall	-0.26	-2.1	0.04

Table 6: Regions with significant differences in $\log(L_P)$ between old and young groups as tested through a t-statistic. All tests were done using the marginal means of $\log(L_P)$ for each brain region as predicted by mixed-effects regression. The "Estimate" column shows the difference in estimated $\log(L_P)$ between 'old' and 'young' groups. All listed regions had p-values below an adjusted alpha calculated using the Benjamini-Hochberg method.

Region	**Estimate**	**t-statistic**	**p-value**
L-Amyg	-0.6	-3.9	0.01
L-Ent	-0.6	-4.0	0.01
L-OrlFG	-0.6	-4.0	0.01
L-Pins	-0.6	-3.9	0.01
R-AntIns	-0.6	-3.8	0.01
R-MPoG	-0.6	-3.8	0.01

R-MPrG	-0.6	-4.1	0.01
L-AntIns	-0.6	-3.7	0.01
L-PO	-0.6	-3.7	0.01
R-OrlFG	-0.6	-3.7	0.01
L-InfLatVent	-0.6	-3.6	0.01
R-TMP	-0.6	-3.6	0.01
L-Gre	-0.6	-3.6	0.01
4th Vent	-0.6	-3.5	0.01
L-Calc	-0.5	-3.3	0.01
L-CerebelEx	-0.5	-3.3	0.01
L-CO	-0.5	-3.4	0.01
L-FO	-0.5	-3.4	0.01
L-PCgG	-0.5	-3.4	0.01
L-PT	-0.5	-3.4	0.01
L-TrlFG	-0.5	-3.3	0.01
L-TTG	-0.5	-3.3	0.01
R-AOrG	-0.5	-3.3	0.01
R-InfLatVent	-0.5	-3.3	0.01
R-LOrG	-0.5	-3.3	0.01
R-PCgG	-0.5	-3.4	0.01
R-Pins	-0.5	-3.3	0.01
R-POrG	-0.5	-3.4	0.01
R-PP	-0.5	-3.4	0.01
L-ACgG	-0.5	-3.2	0.01
Brainstem	-0.5	-3.1	0.01
CerebVermLob VI-VII	-0.5	-3.1	0.01
L-FuG	-0.5	-3.1	0.01
L-Hc	-0.5	-3.2	0.01
L-MFC	-0.5	-3.1	0.01
L-POrG	-0.5	-3.1	0.01
L-PP	-0.5	-3.1	0.01
R-BasForbr	-0.5	-3.1	0.01
R-FO	-0.5	-3.2	0.01
R-ITG	-0.5	-3.1	0.01
L-MOrG	-0.5	-3.0	0.01
L-MPoG	-0.5	-3.1	0.01
L-MPrG	-0.5	-3.0	0.01
L-OFuG	-0.5	-3.1	0.01
L-Putam	-0.5	-3.0	0.01
L-TMP	-0.5	-3.1	0.01
R-OFuG	-0.5	-3.0	0.01
3rd Vent	-0.5	-3.0	0.01
CerebVermLob I-V	-0.5	-2.9	0.02
L-LOrG	-0.5	-3.0	0.02
R-Ent	-0.5	-2.9	0.02

R-Hc	-0.5	-3.0	0.02
R-Pcu	-0.5	-2.9	0.02
R-VentDC	-0.5	-2.9	0.02
R-CO	-0.5	-2.9	0.02
R-Gre	-0.5	-2.9	0.02
L-ITG	-0.5	-2.8	0.02
L-OplFG	-0.5	-2.8	0.02
L-PHG	-0.5	-2.9	0.02
L-SCA	-0.5	-2.8	0.02
L-STG	-0.4	-2.8	0.02
L-VentDC	-0.5	-2.9	0.02
R-LiG	-0.5	-2.8	0.02
R-MOrG	-0.5	-2.8	0.02
L-BasForbr	-0.4	-2.8	0.02
R-CerebelWM	-0.4	-2.8	0.02
R-PHG	-0.4	-2.7	0.02
L-IOG	-0.4	-2.7	0.02
L-MCgG	-0.4	-2.7	0.02
R-MCgG	-0.4	-2.7	0.02
R-PT	-0.4	-2.7	0.02
R-AnG	-0.4	-2.7	0.02
R-MOG	-0.4	-2.7	0.02
L-OCP	-0.4	-2.7	0.02
L-FRP	-0.4	-2.6	0.02
L-LiG	-0.4	-2.6	0.02
R-CerebelEx	-0.4	-2.7	0.02
R-Amyg	-0.4	-2.6	0.02
R-SMC	-0.4	-2.6	0.02
R-STG	-0.4	-2.6	0.02
L-AnG	-0.4	-2.6	0.02
CerebVermLob VII-X	-0.4	-2.6	0.02
R-SCA	-0.4	-2.6	0.02
L-MSFG	-0.4	-2.6	0.02
L-MTG	-0.4	-2.6	0.02
R-ThalProp	-0.4	-2.5	0.02
L-CerebelWM	-0.4	-2.5	0.02
L-CerebWM	-0.4	-2.5	0.02
R-FuG	-0.4	-2.5	0.02
R-IOG	-0.4	-2.5	0.02
L-AcA	-0.4	-2.5	0.02
L-SMG	-0.4	-2.5	0.02
R-CerebWM	-0.4	-2.5	0.03
L-PrG	-0.4	-2.5	0.03
L-ThalProp	-0.4	-2.5	0.03
L-AOrG	-0.4	-2.4	0.03

R-PoG	-0.4	-2.4	0.03
R-OplFG	-0.4	-2.4	0.03
R-Cun	-0.4	-2.4	0.03
L-Pcu	-0.4	-2.3	0.03
R-MFC	-0.4	-2.3	0.04
R-TTG	-0.4	-2.3	0.04
R-SOG	-0.4	-2.3	0.04
L-Cun	-0.4	-2.3	0.04
R-SMG	-0.4	-2.2	0.04
R-MSFG	-0.4	-2.2	0.04
R-PrG	-0.3	-2.2	0.04

Table 7: Regions with significant differences in $\log(B_P)$ between old and young groups as tested through a t-statistic. All tests were done using the marginal means of $\log(B_P)$ for each brain region as predicted by mixed-effects regression. The "Estimate" column shows the difference in estimated $\log(B_P)$ between 'old' and 'young' groups. All listed regions had p-values below an adjusted alpha calculated using the Benjamini-Hochberg method.

3rd Vent	3rd-Ventricle
4th Vent	4th-Ventricle
R-AcA	Right-Accumbens-Area
L-AcA	Left-Accumbens-Area
R-Amyg	Right-Amygdala
L-Amyg	Left-Amygdala
Brainstem	Brain-Stem
R-Caud	Right-Caudate
L-Caud	Left-Caudate
R-CerebelEx	Right-Cerebellum-Exterior
L-CerebelEx	Left-Cerebellum-Exterior
R-CerebelWM	Right-Cerebellum-White-Matter
L-CerebelWM	Left-Cerebellum-White-Matter
R-CerebWM	Right-Cerebral-White-Matter
L-CerebWM	Left-Cerebral-White-Matter
R-Hc	Right-Hippocampus
L-Hc	Left-Hippocampus
R-InfLatVent	Right-Inf-Lat-Vent
L-InfLatVent	Left-Inf-Lat-Vent
R-LatVent	Right-Lateral-Ventricle
L-LatVent	Left-Lateral-Ventricle
R-Pall	Right-Pallidum
L-Pall	Left-Pallidum
R-Putam	Right-Putamen
L-Putam	Left-Putamen
R-ThalProp	Right-Thalamus-Proper
L-ThalProp	Left-Thalamus-Proper
R-VentDC	Right-Ventral-DC
L-VentDC	Left-Ventral-DC
CerebVermLob I-V	Cerebellar-Vermal-Lobules-I-V
CerebVermLob VI-VII	Cerebellar-Vermal-Lobules-VI-VII
CerebVermLob VII-X	Cerebellar-Vermal-Lobules-VIII-X
L-BasForbr	Left-Basal-Forebrain
R-BasForbr	Right-Basal-Forebrain
R-ACgG	Right-ACgG–anterior-cingulate-gyrus
L-ACgG	Left-ACgG–anterior-cingulate-gyrus
R-AntIns	Right-AIns–anterior-insula
L-AntIns	Left-AIns–anterior-insula
R-AOrG	Right-AOrG–anterior-orbital-gyrus
L-AOrG	Left-AOrG–anterior-orbital-gyrus
R-AnG	Right-AnG—angular-gyrus
L-AnG	Left-AnG—angular-gyrus
R-Calc	Right-Calc–calcarine-cortex
L-Calc	Left-Calc–calcarine-cortex
R-CO	Right-CO—-central-operculum

L-CO	Left-CO—-central-operculum
R-Cun	Right-Cun—cuneus
L-Cun	Left-Cun—cuneus
R-Ent	Right-Ent—entorhinal-area
L-Ent	Left-Ent—entorhinal-area
R-FO	Right-FO—-frontal-operculum
L-FO	Left-FO—-frontal-operculum
R-FRP	Right-FRP—frontal-pole
L-FRP	Left-FRP—frontal-pole
R-FuG	Right-FuG—fusiform-gyrus
L-FuG	Left-FuG—fusiform-gyrus
R-Gre	Right-GRe—gyrus-rectus
L-Gre	Left-GRe—gyrus-rectus
R-IOG	Right-IOG—inferior-occipital-gyrus
L-IOG	Left-IOG—inferior-occipital-gyrus
R-ITG	Right-ITG—inferior-temporal-gyrus
L-ITG	Left-ITG—inferior-temporal-gyrus
R-LiG	Right-LiG—lingual-gyrus
L-LiG	Left-LiG—lingual-gyrus
R-LOrG	Right-LOrG–lateral-orbital-gyrus
L-LOrG	Left-LOrG–lateral-orbital-gyrus
R-MCgG	Right-MCgG–middle-cingulate-gyrus
L-MCgG	Left-MCgG–middle-cingulate-gyrus
R-MFC	Right-MFC—medial-frontal-cortex
L-MFC	Left-MFC—medial-frontal-cortex
R-MFG	Right-MFG—middle-frontal-gyrus
L-MFG	Left-MFG—middle-frontal-gyrus
R-MOG	Right-MOG—middle-occipital-gyrus
L-MOG	Left-MOG—middle-occipital-gyrus
R-MOrG	Right-MOrG–medial-orbital-gyrus
L-MOrG	Left-MOrG–medial-orbital-gyrus
R-MPoG	Right-MPoG–postcentral-gyrus
L-MPoG	Left-MPoG–postcentral-gyrus
R-MPrG	Right-MPrG–precentral-gyrus
L-MPrG	Left-MPrG–precentral-gyrus
R-MSFG	Right-MSFG–superior-frontal-gyrus
L-MSFG	Left-MSFG–superior-frontal-gyrus
R-MTG	Right-MTG—middle-temporal-gyrus
L-MTG	Left-MTG—middle-temporal-gyrus
R-OCP	Right-OCP—occipital-pole
L-OCP	Left-OCP—occipital-pole
R-OFuG	Right-OFuG–occipital-fusiform-gyrus
L-OFuG	Left-OFuG–occipital-fusiform-gyrus
R-OplFG	Right-OpIFG-opercular-part-of-the-IFG
L-OplFG	Left-OpIFG-opercular-part-of-the-IFG

R-OrlFG	Right-OrIFG-orbital-part-of-the-IFG
L-OrlFG	Left-OrIFG-orbital-part-of-the-IFG
R-PCgG	Right-PCgG–posterior-cingulate-gyrus
L-PCgG	Left-PCgG–posterior-cingulate-gyrus
R-Pcu	Right-PCu—precuneus
L-Pcu	Left-PCu—precuneus
R-PHG	Right-PHG—parahippocampal-gyrus
L-PHG	Left-PHG—parahippocampal-gyrus
R-Pins	Right-PIns–posterior-insula
L-Pins	Left-PIns–posterior-insula
R-PO	Right-PO—-parietal-operculum
L-PO	Left-PO—-parietal-operculum
R-PoG	Right-PoG—postcentral-gyrus
L-PoG	Left-PoG—postcentral-gyrus
R-POrG	Right-POrG–posterior-orbital-gyrus
L-POrG	Left-POrG–posterior-orbital-gyrus
R-PP	Right-PP—-planum-polare
L-PP	Left-PP—-planum-polare
R-PrG	Right-PrG—precentral-gyrus
L-PrG	Left-PrG—precentral-gyrus
R-PT	Right-PT—-planum-temporale
L-PT	Left-PT—-planum-temporale
R-SCA	Right-SCA—subcallosal-area
L-SCA	Left-SCA—subcallosal-area
R-SFG	Right-SFG—superior-frontal-gyrus
L-SFG	Left-SFG—superior-frontal-gyrus
R-SMC	Right-SMC—supplementary-motor-cortex
L-SMC	Left-SMC—supplementary-motor-cortex
R-SMG	Right-SMG—supramarginal-gyrus
L-SMG	Left-SMG—supramarginal-gyrus
R-SOG	Right-SOG—superior-occipital-gyrus
L-SOG	Left-SOG—superior-occipital-gyrus
R-SPL	Right-SPL—superior-parietal-lobule
L-SPL	Left-SPL—superior-parietal-lobule
R-STG	Right-STG—superior-temporal-gyrus
L-STG	Left-STG—superior-temporal-gyrus
R-TMP	Right-TMP—temporal-pole
L-TMP	Left-TMP—temporal-pole
R-TrlFG	Right-TrIFG-triangular-part-of-the-IFG
L-TrlFG	Left-TrIFG-triangular-part-of-the-IFG
R-TTG	Right-TTG—transverse-temporal-gyrus
L-TTG	Left-TTG—transverse-temporal-gyrus

Table 8: Definition of the brain region labels used in the figures.

References

[1] Carlos López-Otín, Maria A Blasco, Linda Partridge, Manuel Serrano, and Guido Kroemer. The hallmarks of aging. *Cell*, 153(6):1194–1217, 2013.

[2] Hanzhang Lu, Feng Xu, Karen M Rodrigue, Kristen M Kennedy, Yamei Cheng, Blair Flicker, Andrew C Hebrank, Jinsoo Uh, and Denise C Park. Alterations in cerebral metabolic rate and blood supply across the adult lifespan. *Cerebral cortex*, 21(6):1426–1434, 2011.

[3] Douglas N Greve, David H Salat, Spencer L Bowen, David Izquierdo-Garcia, Aaron P Schultz, Ciprian Catana, J Alex Becker, Claus Svarer, Gitte M Knudsen, Reisa A Sperling, et al. Different partial volume correction methods lead to different conclusions: an 18f-fdg-pet study of aging. *Neuroimage*, 132:334–343, 2016.

[4] S Neil Vaishnavi, Andrei G Vlassenko, Melissa M Rundle, Abraham Z Snyder, Mark A Mintun, and Marcus E Raichle. Regional aerobic glycolysis in the human brain. *Proceedings of the National Academy of Sciences*, 107(41):17757–17762, 2010.

[5] Manu S Goyal, Andrei G Vlassenko, Tyler M Blazey, Yi Su, Lars E Couture, Tony J Durbin, Randall J Bateman, Tammie L-S Benzinger, John C Morris, and Marcus E Raichle. Loss of brain aerobic glycolysis in normal human aging. *Cell metabolism*, 26(2):353–360, 2017.

[6] Dominika Drulis-Fajdasz, Agnieszka Gizak, Tomasz Wójtowicz, Jacek R Wiśniewski, and Dariusz Rakus. Aging-associated changes in hippocampal glycogen metabolism in mice. evidence for and against astrocyte-to-neuron lactate shuttle. *Glia*, 66(7):1481–1495, 2018.

[7] Luc Pellerin, Giovanni Pellegri, Philippe G Bittar, Yves Charnay, Constantin Bouras, Jean-Luc Martin, Nephi Stella, and Pierre J Magistretti. Evidence supporting the existence of an activity-dependent astrocyte-neuron lactate shuttle. *Developmental neuroscience*, 20(4-5):291–299, 1998.

[8] Ximena Castillo, Katia Rosafio, Matthias T Wyss, Konstantin Drandarov, Alfred Buck, Luc Pellerin, Bruno Weber, and Lorenz Hirt. A probable dual mode of action for both l-and d-lactate neuroprotection in cerebral ischemia. *Journal of cerebral blood flow & metabolism*, 35(10):1561–1569, 2015.

[9] Akinobu Suzuki, Sarah A Stern, Ozlem Bozdagi, George W Huntley, Ruth H Walker, Pierre J Magistretti, and Cristina M Alberini. Astrocyte-neuron lactate transport is required for long-term memory formation. *Cell*, 144(5):810–823, 2011.

[10] Yaeli Lev-Vachnish, Sharon Cadury, Aviva Rotter-Maskowitz, Noa Feldman, Asael Roichman, Tomer Illouz, Alexander Varvak, Raneen Nicola, Ravit Madar, and Eitan Okun. L-lactate promotes adult hippocampal neurogenesis. *Frontiers in neuroscience*, 13:403, 2019.

[11] Pierre J Magistretti and Igor Allaman. Lactate in the brain: from metabolic end-product to signalling molecule. *Nature Reviews Neuroscience*, 19(4):235–249, 2018.

[12] Silvia Mangia, Ivan Tkáč, Rolf Gruetter, Pierre-Francois Van De Moortele, Federico Giove, Bruno Maraviglia, and Kâmil Uğurbil. Sensitivity of single-voxel 1h-mrs in investigating the metabolism of the activated human visual cortex at 7 t. *Magnetic resonance imaging*, 24(4):343–348, 2006.

[13] Yury Koush, Robin A de Graaf, Lihong Jiang, Douglas L Rothman, and Fahmeed Hyder. Functional mrs with j-edited lactate in human motor cortex at 4 t. *NeuroImage*, 184:101–108, 2019.

[14] Yury Koush, Robin A de Graaf, Ron Kupers, Laurence Dricot, Maurice Ptito, Kevin L Behar, Douglas L Rothman, and Fahmeed Hyder. Metabolic underpinnings of activated and deactivated cortical areas in human brain. *Journal of Cerebral Blood Flow & Metabolism*, 41(5):986–1000, 2021.

[15] Casey Y Lee, Hany Soliman, Benjamin J Geraghty, Albert P Chen, Kim A Connelly, Ruby Endre, William J Perks, Chris Heyn, Sandra E Black, and Charles H Cunningham. Lactate topography of the human brain using hyperpolarized 13c-mri. *Neuroimage*, 204:116202, 2020.

[16] Charles H Cunningham, Albert P Chen, Michael Lustig, Brian A Hargreaves, Janine Lupo, Duan Xu, John Kurhanewicz, Ralph E Hurd, John M Pauly, Sarah J Nelson, et al. Pulse sequence for dynamic volumetric imaging of hyperpolarized metabolic products. *Journal of magnetic resonance*, 193(1):139–146, 2008.

[17] Benjamin J Geraghty, Justin YC Lau, Albert P Chen, and Charles H Cunningham. Dual-echo epi sequence for integrated distortion correction in 3d time-resolved hyperpolarized 13c mri. *Magnetic Resonance in Medicine*, 79(2):643–653, 2018.

[18] MATLAB. *version 7.10.0 (R2019b)*. The MathWorks Inc., Natick, Massachusetts, 2019.

[19] Arno Klein and Jason Tourville. 101 labeled brain images and a consistent human cortical labeling protocol. *Frontiers in neuroscience*, 6:171, 2012.

[20] Yuankai Huo, Zhoubing Xu, Yunxi Xiong, Katherine Aboud, Prasanna Parvathaneni, Shunxing Bao, Camilo Bermudez, Susan M Resnick, Laurie E Cutting, and Bennett A Landman. 3d whole brain segmentation using spatially localized atlas network tiles. *NeuroImage*, 194:105–119, 2019.

[21] Mark Jenkinson, Peter Bannister, Michael Brady, and Stephen Smith. Improved optimization for the robust and accurate linear registration and motion correction of brain images. *Neuroimage*, 17(2):825–841, 2002.

[22] Russell V. Lenth. emmeans: Estimated marginal means, aka least-squares means. *R package version 1.7.3*, 2022.

[23] Yoav Benjamini and Yosef Hochberg. Controlling the false discovery rate: a practical and powerful approach to multiple testing. *Journal of the Royal statistical society: series B (Methodological)*, 57(1):289–300, 1995.

[24] R Core Team et al. R: A language and environment for statistical computing. 2013.

[25] Inge Verheggen, Joost JA de Jong, Martin PJ van Boxtel, Ed HBM Gronenschild, Walter M Palm, Alida A Postma, Jacobus FA Jansen, Frans RJ Verhey, and Walter H Backes. Increase in blood–brain barrier leakage in healthy, older adults. *Geroscience*, 42(4):1183–1193, 2020.

[26] Sam E Day, Mikko I Kettunen, Ferdia A Gallagher, De-En Hu, Mathilde Lerche, Jan Wolber, Klaes Golman, Jan Henrik Ardenkjaer-Larsen, and Kevin M Brindle. Detecting tumor response to treatment using hyperpolarized 13 c magnetic resonance imaging and spectroscopy. *Nature medicine*, 13(11):1382, 2007.

[27] James Prichard, Douglas Rothman, Edward Novotny, Ognen Petroff, Takeo Kuwabara, Malcolm Avison, Alistair Howseman, Christopher Hanstock, and Robert Shulman. Lactate rise detected by 1h nmr in human visual cortex during physiologic stimulation. *Proceedings of the National Academy of Sciences of the United States of America*, 88(13):5829, 1991.

[28] Klaus-Dietmar Merboldt, Harald Bruhn, Wolfgang Hanicke, Thomas Michaelis, and Jens Frahm. Decrease of glucose in the human visual cortex during photic stimulation. *Magnetic resonance in medicine*, 25(1):187–194, 1992.

[29] Igor D Grachev and A Vania Apkarian. Chemical heterogeneity of the living human brain: a proton mr spectroscopy study on the effects of sex, age, and brain region. *Neuroimage*, 11(5):554–563, 2000.

[30] Matthew E Merritt, Crystal Harrison, Charles Storey, F Mark Jeffrey, A Dean Sherry, and Craig R Malloy. Hyperpolarized 13c allows a direct measure of flux through a single enzyme-catalyzed step by nmr. *Proceedings of the National Academy of Sciences*, 104(50):19773–19777, 2007.